SCIENCE CHINA
Technological Sciences

Special Topic: China Seismo-Electromagnetic Satellite
• Article •

https://doi.org/10.1007/s11431-018-9234-9

The HEPD particle detector of the CSES satellite mission for investigating seismo-associated perturbations of the Van Allen belts

AMBROSI Giovanni[1], BARTOCCI Simona[2,3], BASARA Laurent[4], BATTISTON Roberto[5,4], BURGER William J.[4], CARFORA Luca[6,3], CASTELLINI Guido[7], CIPOLLONE Piero[3], CONTI Livio[2,3*], CONTIN Andrea[8,9], DE DONATO Cinzia[3], DE SANTIS Cristian[3], FOLLEGA Francesco M.[5,4], GUANDALINI Cristina[9], IONICA Maria[1], IUPPA Roberto[5,4], LAURENTI Giuliano[9], LAZZIZZERA Ignazio[5,4], LOLLI Mauro[9], MANEA Christian[4], MARCELLI Laura[3], MASCIANTONIO Giuseppe[3], MERGÉ Matteo[3], OSTERIA Giuseppe[10], PACINI Lorenzo[7], PALMA Francesco[6,3], PALMONARI Federico[8,9], PANICO Beatrice[10], PATRIZII Laura[9], PERFETTO Francesco[10], PICOZZA Piergiorgio[6,3], POZZATO Michele[9], PUEL Matteo[4], RASHEVSKAYA Irina[4], RICCI Ester[5,4], RICCI Marco[11], RICCIARINI Sergio Bruno[7], SCOTTI Valentina[10], SOTGIU Alessando[3], SPARVOLI Roberta[6,3], SPATARO Bruno[11] & VITALE Vincenzo[3,12]

[1] *Istituto Nazionale di Fisica Nucleare (INFN), Sezione di Perugia, Perugia 06123, Italy;*
[2] *Uninettuno University, Rome 00186, Italy;*
[3] *Istituto Nazionale di Fisica Nucleare (INFN), Sezione di Roma Tor Vergata, Rome 00133, Italy;*
[4] *Istituto Nazionale di Fisica Nucleare (INFN), TIFPA, Povo (TN) 38123, Italy;*
[5] *Dipartimento di Fisica, Università di Trento, Povo (TN) 38123, Italy;*
[6] *Dipartimento di Fisica, Università di Roma Tor Vergata, Rome 00133, Italy;*
[7] *IFAC-CNR, Sesto Fiorentino (FI) 50019, Italy;*
[8] *Dipartimento di Fisica e Astronomia, Università di Bologna, Bologna 40127, Italy;*
[9] *Istituto Nazionale di Fisica Nucleare (INFN), Sezione di Bologna, Bologna 40127, Italy;*
[10] *Istituto Nazionale di Fisica Nucleare (INFN), Sezione di Napoli, Naples 80126, Italy;*
[11] *Istituto Nazionale di Fisica Nucleare (INFN), LNF, Frascati (RM) 00044, Italy;*
[12] *Agenzia Spaziale Italiana (ASI), SSDC, Rome 00133, Italy*

Received February 6, 2018; accepted March 14, 2018; published online April 11, 2018

CSES (China Seismo-Electromagnetic Satellite) is a mission developed by CNSA (Chinese National Space Administration) and ASI (Italian Space Agency), to investigate the near-Earth electromagnetic, plasma and particle environment, for studying the seismo-associated disturbances in the ionosphere-magnetosphere transition zone. The anthropogenic and electromagnetic noise, as well as the natural non-seismic electromagnetic emissions is mainly due to tropospheric activity. In particular, the mission aims to confirming the existence of possible temporal correlations between the occurrence of earthquakes for medium and strong magnitude and the observation in space of electromagnetic perturbations, plasma variations and precipitation of bursts with high-energy charged particles from the inner Van Allen belt. In this framework, the high energy particle detector (HEPD) of the CSES mission has been developed by the Italian LIMADOU Collaboration. HEPD is an advanced detector based on a tower of scintillators and a silicon tracker that provides good energy and angular resolution and a wide angular acceptance, for electrons of 3–100 MeV, protons of 30–200 MeV and light nuclei up to the oxygen. CSES satellite has been launched on February 2nd, 2018 from the Jiuquan Satellite Launch Center (China).

earthquake, seismic-precursors, particle detector, Van Allen belts, magnetosphere, ionosphere, space weather, cosmic rays

* Corresponding author (email: livio.conti@uninettunouniversity.net)

Citation: Ambrosi G, Bartocci S, Basara L, et al. The HEPD particle detector of the CSES satellite mission for investigating seismo-associated perturbations of the Van Allen belts. Sci China Tech Sci, 2018, https://doi.org/10.1007/s11431-018-9234-9

1 Introduction

The lithosphere dynamics is the result of the stress redistribution among the plates, driven by the mantle convection consequent to the heat released from the deep Earth's interior. Geo-dynamic processes, although permanently act on long temporal scales, can suddenly generate large ruptures. Breaking crustal rocks at the fault asperities that originate the earthquakes, releasing huge amount of mechanical energy and heat [1, 2]. It has also been shown that rock micro fracturing in the Earth's crust—preceding a seismic rupture—can cause not only mechanical effects (such as local surface deformation fields, rock dislocations, fluid diffusion, etc.), but also electromagnetic phenomena (such as activation of charge carriers, changes of electrical conductivity, electrokinetic, piezomagnetic and piezoelectric processes), gas emission, thermal perturbations, etc. [3–8]. These mechanisms are considered as possible sources of the broadband (from DC to a few tens of MHz) electromagnetic emissions, observed at the Earth's surface, in the ionosphere and the inner magnetosphere before, during and after the occurrence of several earthquakes [9, 10]. Starting with the Chile earthquake of 1960 (the largest earthquake ever instrumentally recorded) and the Good Friday earthquake in Alaska of 1964, several seismo-induced ionospheric perturbations have been reported [11, 12]. In occasion of other strong earthquakes, ground-based measurements reveal many electromagnetic phenomena, such as slow electro telluric and magnetic field variations [13], low-frequency (ULF/ELF) electromagnetic signals [14–17] and disturbances in a large (ULF-HF) frequency band [18–21]. A review on the subject, even though not exhaustive, can be found in refs. [22–26]. Characteristic sizes of the preparation focal zone and of the precursor area have been estimated by refs. [27, 28]. Electromagnetic, plasma and particle perturbations detected on board low-Earth orbit (LEO) satellites have also been correlated with seismic activity [29–34] and/or volcanic eruptions [35, 36]. Also thermal anomalies before earthquake have been widely studied with satellite data [37–39]. Moreover, seismo-electromagnetic disturbances can induce particle precipitations from the inner Van Allen belt [40], variations of plasma parameters, fluctuation of total electron content, etc. [41–45]. Anyway, the estimated intensity of the variation of the electric and magnetic field components at LEO altitude is very low: some fractions of $\mathrm{mV/m}\sqrt{\mathrm{Hz}}$ and $\mathrm{nT}/\sqrt{\mathrm{Hz}}$, respectively [34, 46]. What causes, in space, the reported perturbations of so many different parameters is still intensely debated. A direct propagation of seismo-induced electromagnetic signals from the depth up to the upper ionosphere, appears less convincing, due to the strong attenuation occurring in the crust layers, as well as through the atmosphere and the ionospheric plasma. In recent years, interest has been increasing in the so-called lithosphere-atmosphere-ionosphere coupling (LAIC) mechanisms [47]. Nevertheless, up to now, lacks the demonstration of a clear causal relationship between observations and seismic processes and of the correlation between data gathered (simultaneously and continuously) in space and on ground. At this purpose, several projects have been proposed (e.g., ESPERIA [48, 49]) and some of them already launched (DEMETER [50], LAZIO-EGLE[1] [51, 52]), ARINA [53], etc.) or scheduled (e.g., TARANIS, whose main scientific objective is the study of thunderstorm activity and the associated Transient Luminous Events [54]). The main problem in these studies is that have long temporal series of observations and the filtering of data from spurious effects (such as atmospheric electromagnetic emissions during thunderstorm activity and perturbations induced by sun, cosmic rays, etc.). The CSES satellite (also known as Zhangheng-1 (or ZH-1)[2)3)]) [55], with an advanced multi-instrument payload, aims at extending the exploratory study of seismo-electromagnetic phenomena, which is carried out in space by the DEMETER mission. In this article, the high-energy particle detector of the CSES satellite, designed for investigating seismo-induced particles perturbations, is described.

2 Seismo-induced perturbations of the inner Van Allen belt

Particles trapped in the geomagnetic field lines of the Van Allen belts execute gyro-motion, bouncing and longitudinal drift (see Figure 1) according with their adiabatic invariants [56]. Charged particles gyrate around a field line (in opposite directions for negative and positive particles) with a period that depends on the magnetic field strength and the mass of the particle: stronger the magnetic field is, shorter the gyro-period is; heavier the particle is, longer the gyro-period is. The bounce motion occurs, in function of the particle kinetic

1) http://people.roma2.infn.it/~lazio/html/lazio_flight.php.
2) The satellite is named after Zhang Heng, a renowned scholar of the Han Dynasty, who pioneered earthquake studies by inventing the first seismoscope.
3) http://cses.roma2.infn.it/instruments.

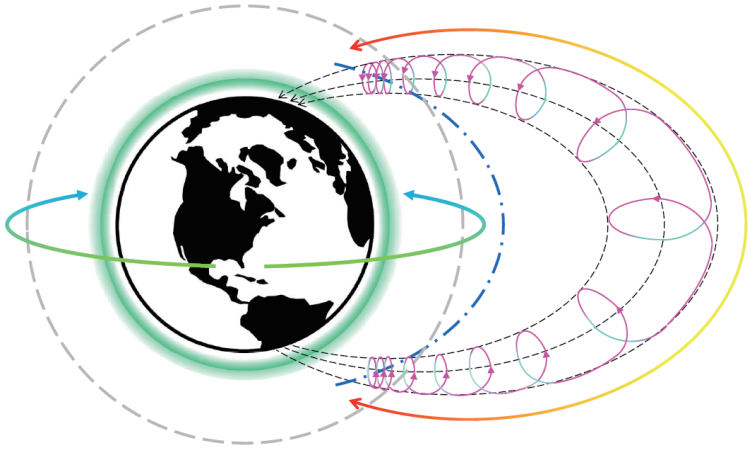

Figure 1 Schematic representation of the particle is trapped by the geomagnetic field. You can see: geomagnetic field lines (black thin dashed lines); gyromotion of trapped particle along the geomagnetic field lines (cyan-magenta curly line); bouncing between the conjugate points (red-yellow line); West-East (East-West) longitudinal drift of the negative (positive) particles (green-blue lines); lower boundary of the inner radiation belt (dot-dashed line blue line); ionosphere (green halo); mirror points/geomagnetic conjugate points (cyan-magenta circles at the endpoints of the bouncing trajectory); low-altitude satellite orbit (grey dashed line).

energy, back and forth along a field line between two mirror points. Faster a particle is, shorter the bounce period is. Particles perform also a slow longitudinal drift around the Earth: electrons drift eastward while charged particles drift westward.

The drift period that is function of the energy and pitch angle of the particles, is of the order of several tens of minutes for electrons and protons of several tens of MeV [56]. Van Allen trapped particles are sensitive to both solar-terrestrial interactions [57, 58], and the internal electromagnetic emissions from the geomagnetic cavity [59]. All these effects constitute a background in studying possible electromagnetic perturbations induced by lithospheric processes. Even though with extremely less efficacious effects, also the seismo-electromagnetic fluctuations occurring in space are capable to generate local perturbations of the inner Van Allen belt. Anomalous sharp increases of electron and proton counting rates (from a few MeV to several tens and hundreds of MeV) were detected mostly below the inner Van Allen radiation belt, near the South Atlantic anomaly (SAA), at altitudes of about 400–1200 km, by several space experiments such as MARIA on board the SALYUT7 station [60], MARIA-2 on the MIR, and the ELECTRON detectors of the INTERCOSMOS BULGARIA-1300 and METEOR-3 satellites [40, 61]. The existence of a temporal correlation between these anomalous fluctuations, called particle bursts (PBs), and the occurrence of earthquakes of medium and strong magnitude have been suggested by several authors [40, 61–64] and confirmed by data obtained on board of METEOR-3A and AUREOL-3 satellites [65, 66]. Statistical analyses [67, 68] confirmed that the detection of such PBs statistically precedes of 2–5 h the occurrence of seismic events. More recently, the same methodology has been applied to analyze more than ten years of 0.3 MeV electron data from several NOAA-POES satellites [69, 70] and the character of PBs as a short time (a few hours) seismic-precursor has been confirmed. It is worth to note that, in the VLF range 1–20 kHz, a direct electromagnetic seismic precursor, consisting in a decrease of the power spectrum intensity for emissions of about 1–2 kHz, has been reported [71] to precede statistically strong earthquakes of about 0–4 h. Several authors [63,65,72] proposed that seismo-induced electromagnetic disturbances in the ionosphere-magnetosphere transition zone (independently by the not yet understood generation and propagation mechanisms) occur at an altitude corresponding to the so called earthquake's L-shell[4)] (possibly function of the frequency of the electromagnetic disturbances, local conditions, etc.), where they can produce a pitch angle diffusion of the trapped particles, inducing their precipitation. After the interaction, precipitating PBs continue their longitudinal drift along the same L-shell, so that they can be detected by satellite not only on the epicentral area of the incoming earthquake, but also at different longitude around the Earth. Positive PBs-EQs time correlations have been obtained also for large distances between the point of the particles detection and the supposed epicentres, in agreement with this hypothesis. The opposite drift direction of positive and negative charged particles could allow reconstructing the longitude of the area (in space) where the injection of particles occurred. Whether this model is valid, this information, together with the latitude of the satellite at time of the PB detection, could allow reconstructing the earthquake prepa-

4) McIlwain L-parameter [73].

ration zone (on ground). In all the above-cited studies of PBs-EQs correlation, PBs has been selected from count rates detected outside the SAA. In fact, due to the structure of the geomagnetic field lines, the particle flux inside the SAA increases several orders of magnitude overwhelming other effects, such as seismo-associated disturbances and does not allow distinguishing between stably trapped particles and perturbed/precipitating ones.

Therefore, observations inside the SAA have been discarded in the analyses. We highlight that, although some seismo-electromagnetic phenomena have a very interesting and promising nature as short-term earthquake precursors, a standard methodology for testing claimed correlations and a deeper knowledge of the physical mechanisms of the earthquake are still lacking. In order to point out the phenomena induced by the seismic activity we need to reject those due to non-seismic disturbances.

3 Background of the Van Allen belt perturbations induced by non-seismic sources

The Van Allen belts are exposed to the influence of many disturbances from Sun and sources internal to the geomagnetic cavity. Geomagnetic storms due to the ejection of high-speed plasma streams associated to solar flare activity generate significant electromagnetic disturbances and strongly influence the dynamics of the Van Allen belts. Electron precipitation has been reported in association with auroral events, chorus, ELF/VLF waves, etc. [74–76]. Geomagnetic (Kp, Ap, Dst, etc.) and solar activity (SID) indices can be useful in monitoring geomagnetic disturbances and for excluding CRs data gathered in disturbed conditions [68–70]. On the other side, the main source of electromagnetic emissions in the near-Earth environment is phenomena, associated to tropospheric activity and more specifically lightning that generates whistlers, right-hand polarized VLF waves which are able to propagate along the geomagnetic field lines from the atmosphere up to the magnetosphere. Resonant interactions between whistlers and gyrating electrons of a few hundreds of keV, which are forced into the loss cone, can cause whistler-induced electron precipitations [77–79]. Finally, an important source of electromagnetic perturbations in the near-Earth space is constituted by anthropogenic emitters, such as power line harmonic radiation, VLF (10–20 kHz) transmitters for radio-navigation and communications, HF broadcasting stations, etc., that can produce electron precipitation [80–82]. Moreover, precipitation of energetic electrons by anthropogenic waves may trigger other lightning discharges. In the framework of our investigation of the seismo-induced effects on the trapped particles, a deep investigation and the rejection of all these background events are a precondition for any study of seismo-associated phenomena, because the ionospheric and magnetospheric disturbances may lead to misinterpretations in many cases.

4 The CSES mission and the LIMADOU collaboration

Even though forecasting of earthquakes is not possible nowadays, the investigation of seismic precursors from space represents a challenge and an opportunity to improve knowledge of the physics of the earthquake. In order to investigate seismo-associated phenomena, it needs a multi-instrument satellite, which is able to detect simultaneously several physical parameters. In this context, the CSES mission is a joint collaboration between the China National Space Agency (CNSA) and the Italian Space Agency (ASI). The Chinese research team, including several universities and research institutes, is led by the China Earthquake Administration (CEA). The Italian participation to CSES, called LIMADOU project—after the Chinese name of the missionary Matteo Ricci who explored China in the 16th century [83]—includes teams from the Italian National Institute of Nuclear Physics (INFN), the Universities of Bologna, Roma Tor Vergata, Trento, Uninettuno, the National Institute for Astrophysics (INAF) and the National Institute of Geophysics and Volcanology (INGV). CSES mission aims at improving the observations in order to clarify the long-standing question of the existence, nature and rate of occurrence of seismo-associated phenomena better. Another very important and scientific objective is the study of the solar-terrestrial environment, solar impulsive activity (e.g., solar energetic particle (SEP) events) and solar modulation of low-energy cosmic rays in the electron and proton energy range from few MeV to hundreds MeV. These measurements will provide an extension up to very low energy of the particle spectra obtained in the current 24th solar cycle by PAMELA [84] and AMS [85] experiments. CSES observations will allow comparing particle spectra with those from GOES and ACE missions. Moreover, fluxes of light nuclei up to hundreds MeV/n will be provided. CSES is a 3-axis attitude stabilized satellite, which is based on the Chinese CAST2000 platform (see Figure 2 and 3) of the DFH Satellite Co. Ltd. (Beijing, China)[5)], with a mass of about 730 kg and a peak power consumption of about 900 W. The orbit is Sun-synchronous with 97.4° inclination, at an altitude of 507 km for an expected mission lifetime greater than 5 years. The CSES payload consists of nine instruments[3)]. Two devices, the high-energy particle detectors (HEPD) and

5) http://www.cast.cn/Item/list.asp?id=1814.

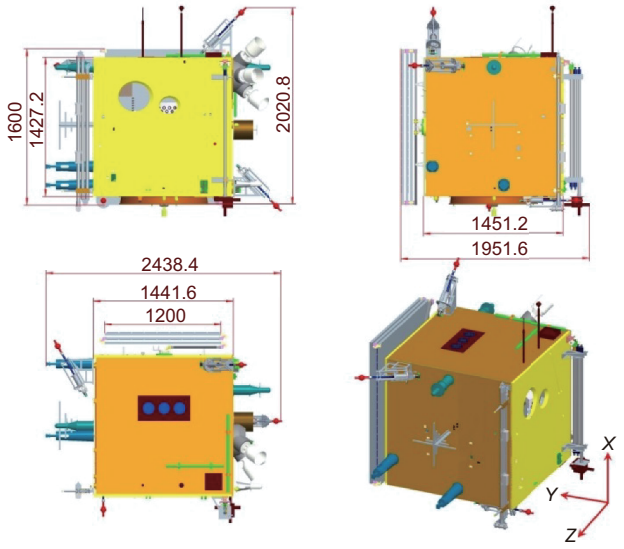

Figure 2 Several views of the CSES layout with the 4 telescopic booms of the EFD probes stowed. The search-coil magnetometer boom is folded at the edge between the *XZ* and the *XY* planes.

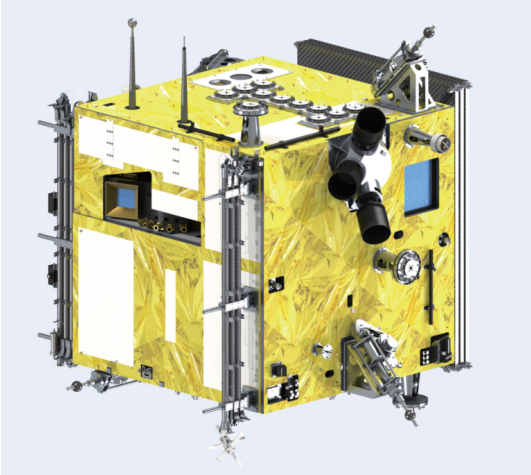

Figure 3 Rendering of the CSES satellite. On the right face of the platform (i.e. the panel of the satellite pointing to zenith) near the block of the three star trackers, it is the visible HEPD detection window (blue rectangle).

the high-energy particle package (HEPP), can detect flux and energy of charged particles; a search-coil magnetometer and a high-precision magnetometer will measure components and total intensity of the magnetic field, respectively; an electric field detector (EFD) will register the electric field components. Moreover, a Plasma analyser and a Langmuir probe will register plasma parameters, whereas a GNSS Occultation Receiver and a Tri-Band Beacon the electron density profile. The multi-instrument payload gives the possibility, by measuring simultaneously several different parameters, to better identify the signature of the studied phenomena from many different perspectives and with many details. Scientific data will be gathered and transmitted in the magnetic latitude range of ±65°, whereas at higher latitudes it will be carried out platform pointing adjustments. The LIMADOU Collaboration has conceived and built the innovative detector of particles HEPD and collaborated in testing the advanced EFD instrument [86–88] and the Langmuir probes at the INAF-IAPS's plasma chamber facility in Rome (Italy)[6]. By measuring energy spectrum, direction and composition of particle fluxes, HEPD will study the stability of the inner Van Allen belts and particles precipitation trying to carefully discriminate anomalous events possibly induced by seismicity from the natural background, caused by geomagnetic, tropospheric and anthropogenic electromagnetic emissions. In this framework, EFD can complement the investigation , because while seismo-induced precipitations are an indirect effect of disturbances due to earthquakes, EFD can directly measure the seismo-electromagnetic disturbances.

5 The high energy particle detector

The HEPD instrument, based on the technology of multi-layers silicon particle detectors, is the direct evolution of several experiments built and successfully flown in the past[7] by researchers of the LIMADOU collaboration, such as NINA-1 (1998), NINA-2 (2000), Sileye-1 (1997) and Sileye-2 (1998), ARINA (2006), Pamela (2006), AMS-01 (1998) and AMS-02 (2011), etc. Designed to detect electrons in the energy range between 3 and 100 MeV, protons between 30 and 200 MeV and light nuclei up to oxygen, HEPD is located on the top of the satellite pointing to zenith. The wide energetic and geometrical acceptance factor of the instrument, together with the high inclination of the CSES orbit, allow detecting particles of different nature, such as those trapped in the magnetosphere, low energy component of anomalous cosmic rays and SEP. HEPD is made up of several sub-detectors (see Figure 4):

1) A silicon detector consisting of two double-side silicon micro strip sensor planes (10 mm distant) placed on the top of the HEPD, with a total dimension of 213 mm × 213 mm × 0.3 mm. Each layer is made of 3 ladders, each one composed by 2 modules, 300 μm thick and resolution of 50 μm. The instrument provides direction and energy loss of the incident particle;

2) A plane of plastic scintillator, 10 mm below the silicon detector, segmented into 6 paddles (200 mm × 30 mm × 5 mm each). Each paddle is read out by a photomultiplier tube (PMT R9880-210 from Hamamatsu) on each side;

6) http://www.iaps.inaf.it/downloads/2016-INAF-IAPS-PlasmaChamb.
7) http://wizard.roma2.infn.it.

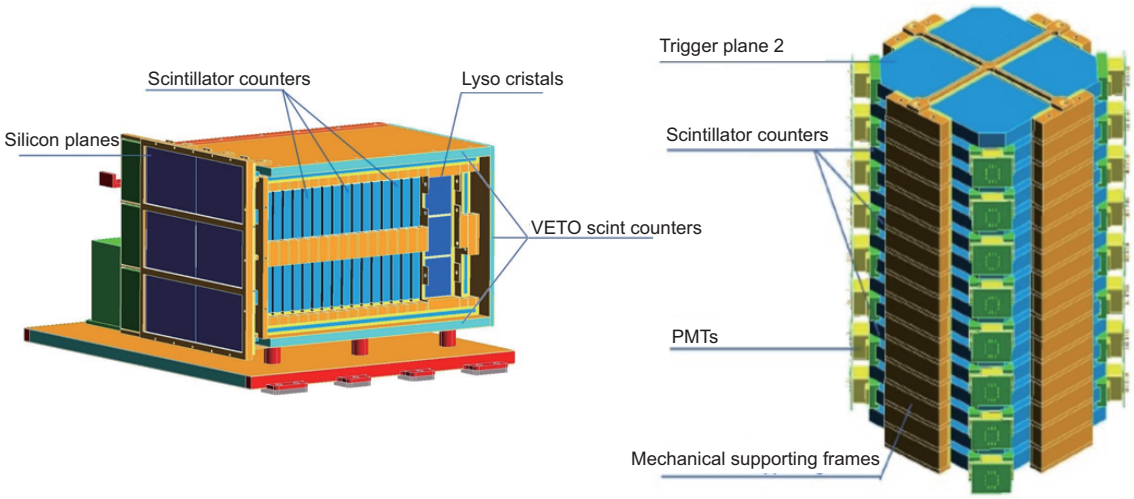

Figure 4 HEPD layout.

3) A range-calorimeter, divided into two sections. Its upper part is a tower of 16 plastic scintillator planes (150 mm × 150 mm × 10 mm), each read out by two PMTs. The lower part of the calorimeter is a 3 × 3 matrix of inorganic scintillators (LYSO). Each crystal (48 mm × 48 mm × 40 mm) is read out by a PMT located on the bottom face;

4) A veto system of 5 plastic scintillator counters, 5 mm thick, four lateral and one at the bottom of the instrument.

A good separation for fully contained particle events is achieved by the ΔE vs $E_{\rm tot}$ method, where ΔE is obtained by the two layers of the silicon tracker, while $E_{\rm tot}$ is measured by the calorimeter. Figure 5 shows the simulated electron/proton separation, while the nuclei separation is shown in Figure 6. The HEPD electronics subsystem (ELS) consists of: a CPU board, to control the whole detector status and to communicate with the platform; a data acquisition board for silicon detector read-out, event processing, compression and formatting during the acquisitions; a trigger board for trigger generation and read-out of the PMT data; a high voltage board, to provide the high voltage for the two silicon planes and the 63 PMTs; a power control board to provide the power supply to all the other components of the ELS. The HEPD detector is contained in a box of aluminium honeycomb. An aluminized polyimide layer covers the outside surface to assure a good thermal insulation. HEPD has mechanical dimensions of 53 cm × 38.2 cm × 40.4 cm, mass of 45 kg and power consumption of 27 W. Other main parameters of HEPD are

Electron energy: 3–100 MeV;

Protons energy: 30–200 MeV;

Nuclei identification: up to oxygen;

Energy resolution: < 10%;

Angular resolution: < 8°;

Field of view: ≃ 60°.

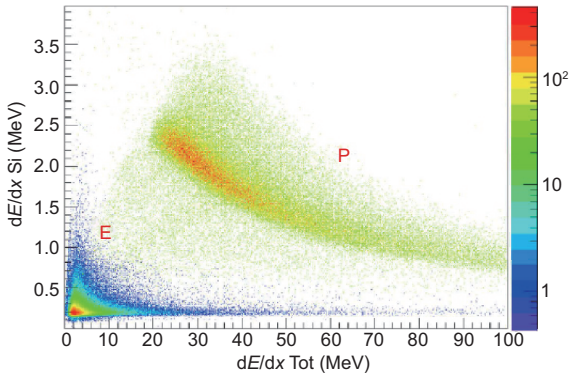

Figure 5 HEPD simulated electron vs proton separation.

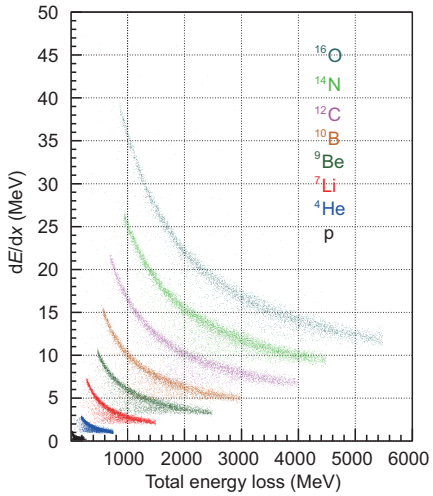

Figure 6 HEPD simulated nuclei separation.

Geometry factor for electrons and protons is shown in Figure 7 in function of the energy. HEPD is able to distinguish type and characteristics of each single charged particle hitting the detector; therefore rate and amount of data recorded along

the orbit vary depending on the particle data rate and the geomagnetic coordinates. For each event, stored data (provided to the scientific community) consist of: type (electron, proton or light nucleus), energy and impact direction of the detected particle, as well as of auxiliary information (such as GPS time, satellite position and speed). HEPD operates within ±65°, for a total data budget up to 50 Gbit per day, as allowed by the CSES memory budget and data transmission constraints. More information on data processing, data products/levels and data policy will be given in a forthcoming article[8].

Following the standard procedures for space applications, four models of HEPD have been built and fully integrated in the clean rooms at the INFN laboratories of Roma Tor Vergata in Rome (Italy). The electrical model (EM), including only the electrical and transmission subsystems, was used in order to validate the wire connections between the payload and the satellite. The structural and thermal model (STM), mechanically equal to the flight instrument, but with dummy sensors and electronics, instead of the real ones, was constructed to validate the structure and mechanical design as well as the thermal conductivity. The qualification model (QM), identical to the flight detector, was used in order to qualify (by stress tests) all the subsystems, calibrate the instrument and assess its compliance with requirements for space applications. Finally, the flight model (FM) was assembled (Figure 8). It underwent not stressing vibration, thermal-cycling and thermal-vacuum tests in Italy before the shipping to China, in December 2016. In January 2017, the functionality of the instrument was successfully tested standalone with its EGSE; then it was installed on the CSES satellite (Figure 9). The random vibration and thermal-vacuum tests were accomplished, in February and April, respectively; while magnetic cleanliness and aging tests in May. Finally, in December 2017, HEPD has been transferred to the Jiuquan Satellite Launch Center, China, in the Gobi desert (Inner Mongolia) from where it has been launched, by a Long March 2D rocket, on the February 2nd, 2018.

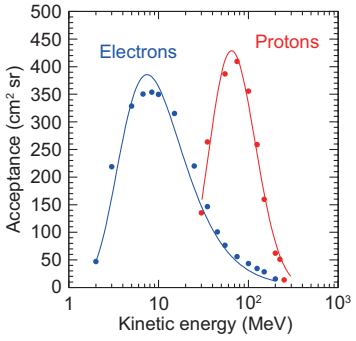

Figure 7 Electron and proton estimated acceptances.

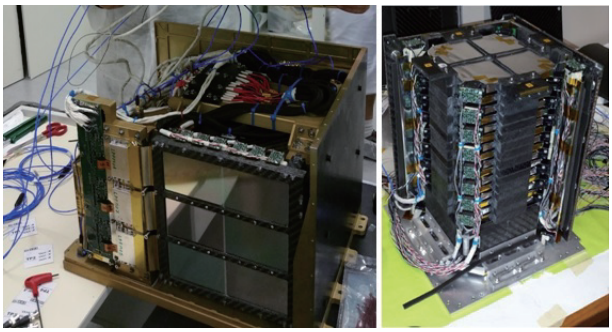

Figure 8 The electronics and the silicon detector of the HEPD-FM (left panel). A side view of the HEPD-QM calorimeter (right panel) with the tower of 16 plastic scintillators and the PMTs at the corners of each calorimeter plane.

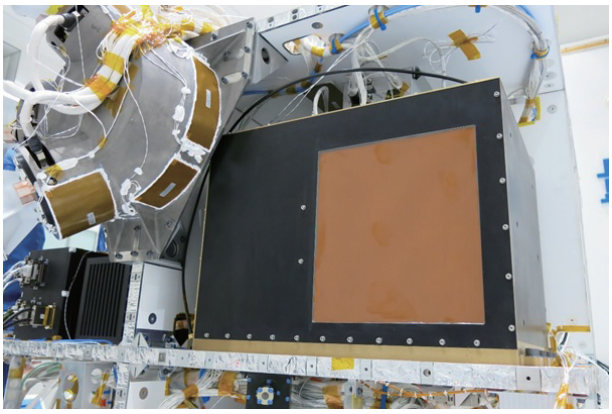

Figure 9 HEPD installed on CSES satellite.

6 HEPD calibration

Calibrations of the HEPD flight model have been performed by electron and proton beams and cosmic muons. Electron beam tests took place at the beam test facility (BTF) of the INFN Frascati National Laboratories. The parameters of the BTF were optimized to obtain beam bunches of low multiplicity (0, 1, > 1 electrons according to a Poisson distribution) for different energies: 30, 45, 60 and 120 MeV. The beam spot radius was 4.9 mm×5.3 mm at 30 MeV. The HEPD was placed in front of the beam on a movable platform. Data collected were transmitted to the EGSE module that was controlled remotely from the control room, so emulating satellite in orbit conditions.

The calibrations have been performed at different incident angles and positions. The total energy loss in the calorimeter for 30 MeV electrons is shown in Figure 10. Peaks corresponding to one, two, three electrons hitting the instrument

8) Conti L. and the CSES-Limadou Collaboration, First results of the HEPD detector of the CSES mission. In preparation.

in a single beam bunch are clearly visible. Protons beam tests have been performed at the Proton Therapy Center in Trento (Italy) in the energy range 37–228 MeV. Protons of energies below 70 MeV have been obtained by using a degrader along the beam. Results for 70 MeV protons are shown in Figure 11. In Figure 12, a comparison between proton beam data and MC simulation for dE/dx measurements is shown. Figure 13 shows the calibration plot of the detector in function of energy.

7 Conclusions

Several observations and related analyses suggested the possibility that precipitation of anomalous particle bursts and electromagnetic fluctuations detected by LEO satellites can be induced by seismo-associated disturbances in the ionosphere-magnetosphere transition zone. The CSES satellite aims at investigating such a phenomena under controlled conditions, and with a suite of advanced instruments conceived, in order to perform simultaneous measurements of many different parameters of the seismo-associated perturbations. In this framework, the Italian LIMADOU collaboration participates to the mission providing the HEPD instrument for measurements of charged particles. The detector has been designed, built and fully tested for measuring electrons in the energy range between 3 and 100 MeV, protons between 30 and 200 MeV and light nuclei up to oxygen. The HEPD configuration represents a substantial improvement (for detector reliability, particle identification, energy range, pitches angle resolution, etc.) with respect to all particle detectors (with similar objectives and energy range) recently launched (such as IDP on Demeter, ARINA, etc.). The wide energetic range allows studying several phenomena beyond the seismo-associated ones, such as those related to magnetospheric currents, dynamics of radiation belts and cosmic rays flux. During the foreseen five years of the mission, a large part of the 24th solar cycle will be monitored.

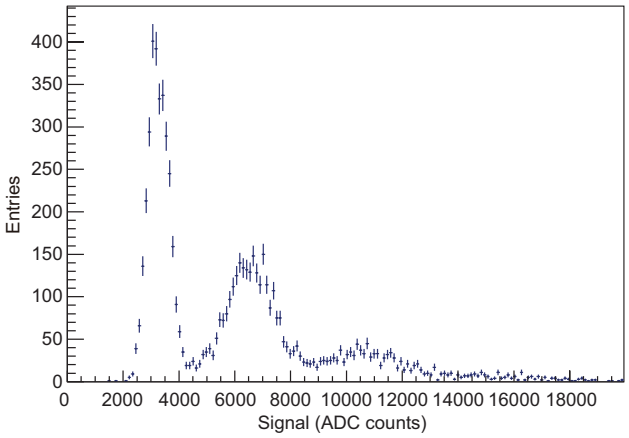

Figure 10 Energy loss by 30 MeV electrons within the upper segment of the HEPD calorimeter. The second and third peaks are produced by the pile-up of 2 or 3 simultaneous electrons.

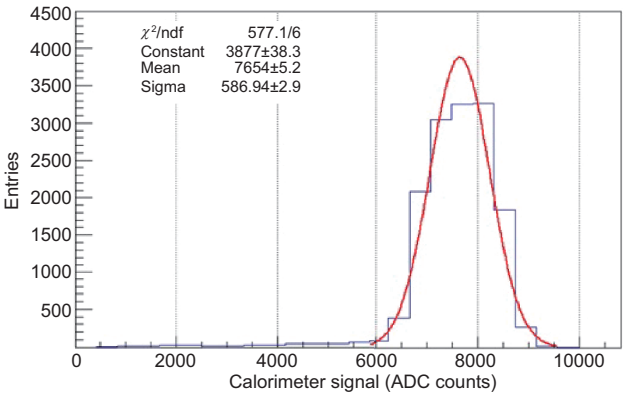

Figure 11 Total energy loss in the HEPD calorimeter for 70 MeV protons. Sigma/peak = 0.08.

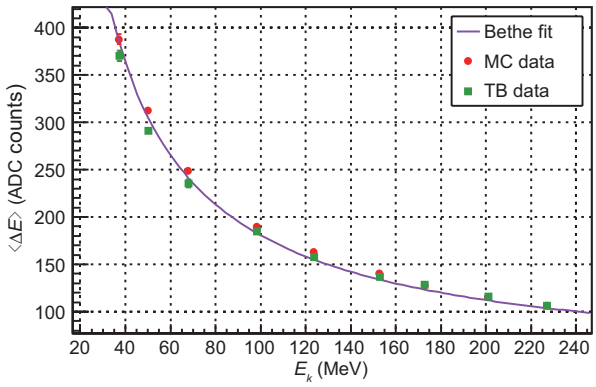

Figure 12 Measured proton dE/dx, for a silicon plane at different energies of the test beam (TB), compared with MC simulation.

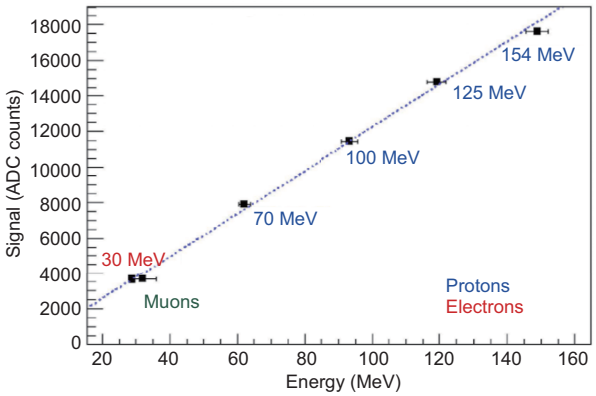

Figure 13 HEPD calibration plot in function of energy.

This work was supported by the Italian Space Agency in the framework of the "Accordo Attuativo n. 2016-16-H0 Progetto Limadou Fase E/Scienza" (CUP F12F1600011005).

1 Lay T, Wallace T C. Modern Global Seismology. San Diego: Academic Press, 1995
2 Mjachkin V I, Brace W F, Sobolev G A, et al. Two models for earthquake forerunners. Pure Appl Geophys, 1975, 113: 169–181
3 Pulinets S, Boyarchuk K. Ionospheric Precursors of Earthquakes. New York: Springer, 2004
4 Cicerone R D, Ebel J E, Britton J. A systematic compilation of earthquake precursors. Tectonophysics, 2009, 476: 371–396
5 Freund F T, Kulahci I G, Cyr G, et al. Air ionization at rock surface and pre-earthquake signals. J Atmos Sol-Terr Phys, 2009, 71: 1824–1834
6 Freund F T. Toward a unified solid state theory for pre-earthquake signals. Acta Geophys, 2010, 58: 719–766
7 Hayakawa M. Earthquake Prediction Studies: Seismo Electromagnetics. Tokyo: Terrapub, 2013. 794
8 Pulinets S A, Ouzounov D P, Karelin A V, et al. Physical bases of the generation of short-term earthquake precursors: A complex model of ionization-induced geophysical processes in the lithosphere-atmosphere-ionosphere-magnetosphere system. Geomagn Aeron, 2015, 55: 521–538
9 Sgrigna V, Buzzi A, Conti L, et al. Seismo-induced effects in the near-earth space: Combined ground and space investigations as a contribution to earthquake prediction. Tectonophysics, 2007, 431: 153–171
10 De Santis A, De Franceschi G, Spogli L, et al. Geospace perturbations induced by the Earth: The state of the art and future trends. Phys Chem Earth Parts A/B/C, 2015, 85-86: 17–33
11 Warwick J W, Stoker C, Meyer T R. Radio emission associated with rock fracture—Possible application to the great Chilean earthquake of May 22, 1960. J Geophys Res, 1982, 87: 2851–2859
12 Davies K, Baker D M. Ionospheric effects observed around the time of the Alaskan Earthquake of March 28, 1964. J Geophys Res, 1965, 70: 2251–2253
13 Varotsos P, Alexopoulos K, Lazaridou-Varotsou M, et al. Earthquake predictions issued in Greece by seismic electric signals since February 6, 1990. Tectonophysics, 1993, 224: 269–288
14 Kopytenko Y A, Matiashvili T G, Voronov P M, et al. Detection of ultra-low-frequency emissions connected with the Spitak earthquake and its aftershock activity, based on geomagnetic pulsations data at Dusheti and Vardzia observatories. Phys Earth Planet Inter, 1993, 77: 85–95
15 Fraser-Smith A C, McGill P R, Helliwell R A, et al. Ultra-low frequency magnetic field measurements in southern California during the Northridge Earthquake of 17 January 1994. Geophys Res Lett, 1994, 21: 2195–2198
16 Ohta K, Umeda K, Watanabe N, et al. ULF/ELF emissions observed in Japan, possibly associated with the Chi-Chi earthquake in Taiwan. Nat Hazards Earth Syst Sci, 2001, 1: 37–42
17 Ismaguilov V S, Kopytenko Y A, Hattori K, et al. ULF magnetic emissions connected with under sea bottom earthquakes. Nat Hazards Earth Syst Sci, 2001, 1: 23–31
18 Oike K, Ogawa T. Electromagnetic radiations from shallow earthquakes observed in the LF range. J Geomagn Geoelec, 1986, 38: 1031–1040
19 Johnston M J S. Review of electric and magnetic fields accompanying seismic and volcanic activity. Surveys Geophys, 1997, 18: 441–476
20 Uyeda S, Al-Damegh K S, Dologlou E, et al. Some relationship between VAN seismic electric signals (SES) and earthquake parameters. Tectonophysics, 1999, 304: 41–55
21 Eftaxias K, Kapiris P, Polygiannakis J, et al. Experience of short term earthquake precursors with VLF-VHF electromagnetic emissions. Nat Hazards Earth Syst Sci, 2003, 3: 217–228
22 Park S K, Johnston M J S, Madden T R, et al. Electromagnetic precursors to earthquakes in the Ulf band: A review of observations and mechanisms. Rev Geophys, 1993, 31: 117–132
23 Merzer M, Klemperer S L. Modeling low-frequency magnetic-field precursors to the Loma Prieta Earthquake with a precursory increase in fault-zone conductivity. Pure Appl Geophys, 1997, 150: 217–248
24 Molchanov O A, Hayakawa M. On the generation mechanism of ULF seismogenic electromagnetic emissions. Phys Earth Planet Inter, 1998, 105: 201–210
25 Surkov V. ULF electromagnetic perturbations resulting from the fracture and dilatancy in the earthquake preparation zone. In: Atmospheric and Ionospheric Electromagnetic Phenomena Associated with Earthquakes. Tokyo: Terrapub, 1999. 371–382
26 Hayakawa M, Kopytenko Y, Smirnova N, et al. Monitoring ULF magnetic disturbances, and schemes for recognizing earthquake precursors. Phys Chem Earth Part A-Solid Earth Geodesy, 2000, 25: 263–269
27 Dobrovolsky I P, Zubkov S I, Miachkin V I. Estimation of the size of earthquake preparation zones. Pure Appl Geophys, 1979, 117: 1025–1044
28 Dobrovolsky I P, Gershenzon N I, Gokhberg M B. Theory of electrokinetic effects occurring at the final stage in the preparation of a tectonic earthquake. Phys Earth Planet Inter, 1989, 57: 144–156
29 Gokhberg M B, Morgounov V A, Aronov E L. On the high frequency electromagnetic radiation during seismic activity. Dokladi Acad Sci USSR, 1979, 248: 1077–1081
30 Larkina V I, Migulin V V, Molchanov O A, et al. Some statistical results on very low frequency radiowave emissions in the upper ionosphere over earthquake zones. Phys Earth Planet Inter, 1989, 57: 100–109
31 Parrot M, Mogilevsky M M. VLF emissions associated with earthquakes and observed in the ionosphere and the magnetosphere. Phys Earth Planet Inter, 1989, 57: 86–99
32 Bilichenko S V, Iljin F S, Kim E F, et al. ULF response of the ionosphere for earthquake preparation processes. Dokl Acad Nauk USSR, 1990, 311: 1077–1080
33 Serebryakova O N, Bilichenko S V, Chmyrev V M, et al. Electromagnetic ELF radiation from earthquake regions as observed by low-altitude satellites. Geophys Res Lett, 1992, 19: 91–94
34 Parrot M, Achache J, Berthelier J J, et al. High-frequency seismo-electromagnetic effects. Phys Earth Planet Inter, 1993, 77: 65–83
35 Zlotnicki J, Li F, Parrot M. Signals recorded by DEMETER satellite over active volcanoes during the period 2004 August-2007 December. Geophys J Int, 2010, 183: 1332–1347
36 Zlotnicki J, Li F, Parrot M. Ionospheric disturbances recorded by DEMETER Satellite over active volcanoes: From August 2004 to December 2010. Int J Geophys, 2013, 2013: 1–17
37 Ouzounov D, Freund F. Mid-infrared emission prior to strong earthquakes analyzed by remote sensing data. Adv Space Res, 2004, 33: 268–273
38 Ouzounov D, Liu D, Chunli K, et al. Outgoing long wave radiation variability from IR satellite data prior to major earthquakes. Tectonophysics, 2007, 431: 211–220
39 Tramutoli V, Cuomo V, Filizzola C, et al. Assessing the potential of thermal infrared satellite surveys for monitoring seismically active areas: The case of Kocaeli (Izmit) earthquake, August 17, 1999. Remote Sens Environ, 2005, 96: 409–426
40 Galper A M, Dmitrenko V V, Nikitina N V, et al. Interrelation of fluxes of high energy charged particles in radiation belt with seismicity of Earth. Cosmic Res, 1989, 27: 789–792
41 Chmyrev V M, Isaev N V, Serebryakova O N, et al. Small-scale plasma inhomogeneities and correlated ELF emissions in the ionosphere over an earthquake region. J Atmos Sol-Terr Phys, 1997, 59: 967–974
42 Rodger C J, Dowden R L, Thomson N R. Observations of electromagnetic activity associated with earthquakes by low altitude satellites. In: Atmospheric and Ionospheric Electromagnetic Phenomena Associated with Earthquakes. Tokyo: Terrapub, 1999, 697–710
43 Yan R, Parrot M, Pinçon J L. Statistical study on variations of the ionospheric ion density observed by DEMETER and related to seismic activities. J Geophys Res Space Phys, 2017, 122: 12421–12429
44 Lee C C, Liu J Y, Pan C J, et al. The heights of sporadic-E layer si-

multaneously observed by the VHF radar and ionosondes in Chung-Li. Geophys Res Lett, 2000, 27: 641–644
45 Parrot M, Berthelier J J, Lebreton J P, et al. Examples of unusual ionospheric observations made by the DEMETER satellite over seismic regions. Phys Chem Earth Parts A/B/C, 2006, 31: 486–495
46 Bortnik J, Bleier T E, Dunson C, et al. Estimating the seismotelluric current required for observable electromagnetic ground signals. Ann Geophys, 2010, 28: 1615–1624
47 Pulinets S, Ouzounov D. Lithosphere-Atmosphere-Ionosphere Coupling (LAIC) model: An unified concept for earthquake precursors validation. J Asian Earth Sci, 2011, 41: 371–382
48 Sgrigna V. Program for scientific missions dedicated to Earth sciences. ESPERIA Phase A Report. Rome: Italian Space Agency (ASI), 2001. 1–194
49 Sgrigna V, Console R, Conti L, et al. The ESPERIA project: A mission to investigate the near-Earth space. In: Earth Observation with CHAMP. Berlin-Heidelberg: Springer, 2005. 407–412
50 Parrot M. The micro-satellite DEMETER. J GeoDyn, 2002, 33: 535–541
51 Bencardino R, Altaura F, Bidoli V, et al. Response of the LAZIO-SiRad detector to low energy electrons. In: Proceedings of the 29th International Cosmic Ray Conference. Mumbai: Tata Institute of Fundamental Research, 2005. 449–452
52 Sgrigna V, Altamura F, Ascani S, et al. First data from the EGLE experiment onboard the ISS. Microgravity Sci Tec, 2007, 19: 70–74
53 Bakaldin A V, Batishchev A G, Voronov S A, et al. Satellite experiment ARINA for studying seismic effects in the high-energy particle fluxes in the Earth's magnetosphere. Cosmic Res, 2007, 45: 445–448
54 Lefeuvre F, Blanc E, Pincçon J L, et al. TARANIS-a satellite project dedicated to the physics of TLEs and TGFs. In: Planetary Atmospheric Electricity. New York: Springer, 2008, 301–315
55 Shen X H, Zhang X M, Wang L W, et al. The earthquake related disturbances in ionosphere and project of the first China seismo-electromagnetic satellite. Earthq Sci, 2011, 24: 639–650
56 Walt M. Introduction to Geomagnetically Trapped Radiation. Cambridge: Cambridge University Press, 1994
57 Lanzerotti L J. Space weather and natural hazards. Space Weather, 2012, 10: S05008
58 Shprits Y Y, Subbotin D, Drozdov A, et al. Unusual stable trapping of the ultrarelativistic electrons in the Van Allen radiation belts. Nat Phys, 2013, 9: 699–703
59 Parrot M, Zaslavski Y. Physical mechanisms of man-made influences on the magnetosphere. Surv Geophys, 1996, 17: 67–100
60 Voronov S A, Galper A M, Koldashov S V, et al. Registration of sporadic increase of high energy particle flux near brazilian anomaly region. In: Proceedings of the 20th International Cosmic Ray Conference Moscow, Volume 4. 1987. 451–452
61 Voronov S A, Galper A M, Koldashov S V, et al. Increase of high-energy charged particle fluxes in SAA region and the Earth's seismic activity. Cosmic Res, 1990, 28: 789–791
62 Voronov S A, Galper A M, Koldashov S V, et al. Observation of high-energy charged particle flux increases in SAA region in 10 September 1985. Cosmic Res, 1989, 27: 629–631
63 Aleshina M E, Galper A M, Koldashov S V, et al. Interrelation between locations of charged particle precipitation regions and earthquake epicentres. Cosmic Res, 1992, 30: 79–81
64 Galper A M, Koldashov S V, Voronov S A. High energy particle flux variations as earthquake predictors. Adv Space Res, 1995, 15: 131–134
65 Galperin Yu I, Gladyshev V A, Jordjio N V, et al. Precipitation of high-energy captured particles in the magnetosphere above epicenter of an incipient earthquake. Cosmic Res, 1992, 30: 89–106
66 Pustovetov V P, Malyshev A V. Spatial-temporal correlation of the earthquakes and variations of high-energy particle flux in the inner radiation belt. Cosmic Res, 1993, 31: 84–87
67 Aleksandrin S Yu, Galper A M, Grishantzeva L A, et al. High-energy charged particle bursts in the near-Earth space as earthquake precursors. Ann Geophys, 2003, 21: 597–602
68 Sgrigna V, Carota L, Conti L, et al. Correlations between earthquakes and anomalous particle bursts from SAMPEX/PET satellite observations. J Atmos Sol-Terr Phys, 2005, 67: 1448–1462
69 Fidani C, Battiston R, Burger W J, et al. A study of NOAA particle flux sensitivity to solar activity and strategies to search for correlations among satellite data and earthquake phenomena. Int J Remote Sens, 2012, 33: 4796–4814
70 Battiston R, Vitale V. First evidence for correlations between electron fluxes measured by NOAA-POES satellites and large seismic events. Nucl Phys B-Proc Sup, 2013, 243-244: 249–257
71 Němec F, Santolík O, Parrot M, et al. Spacecraft observations of electromagnetic perturbations connected with seismic activity. Geophys Res Lett, 2008, 35: L05109
72 Krechetov V V. Cerenkov radiation of protons in the magnetosphere as a source of VLF waves preceding an earthquake. Geomagn Aeron (Engl Transl), 1996, 35: 688–691
73 McIlwain C E. Coordinates for mapping the distribution of magnetically trapped particles. J Geophys Res, 1961, 66: 3681–3691
74 Swift D W. Mechanisms for auroral precipitation—A review. Rev Geophys, 1981, 19: 185–211
75 Walt M, Voss H D, Pickett J. Electron precipitation coincident with ELF/VLF wave bursts. J Geophys Res, 2002, 107: SMP 28-1–SMP 28-6
76 Millan R M, Thorne R M. Review of radiation belt relativistic electron losses. J Atmos Sol-Terr Phys, 2007, 69: 362–377
77 Rodger C J, Clilverd M A, McCormick R J. Significance of lightning generated whistlers to inner radiation belt electron lifetimes. J Geophys Res, 2003, 108: 1462
78 Inan U S, Piddyachiy D, Peter W B, et al. DEMETER satellite observations of lightning-induced electron precipitation. Geophys Res Lett, 2007, 34: L07103
79 Gemelos E S, Inan U S, Walt M, et al. Seasonal dependence of energetic electron precipitation: Evidence for a global role of lightning. Geophys Res Lett, 2009, 36: L21107
80 Sauvaud J A, Maggiolo R, Jacquey C, et al. Radiation belt electron precipitation due to VLF transmitters: Satellite observations. Geophys Res Lett, 2008, 35: L09101
81 Graf K L, Inan U S, Piddyachiy D, et al. DEMETER observations of transmitter-induced precipitation of inner radiation belt electrons. J Geophys Res, 2009, 114: A07205
82 Sauvaud J A, Parrot M, Slominska E. Comment on "Comparative study on earthquake and ground based transmitter induced radiation belt electron precipitation at middle latitude", by Sideropoulos et al. (2011). Nat Hazards Earth Syst Sci, 2014, 14: 1–9
83 Shih J H. Matteo Ricci—Italian Jesuit missionary. In: Encyclopedia Britannica. Https://www.britannica.com/biography/Matteo-Ricci, 2017
84 Picozza P, Galper A M, Castellini G, et al. PAMELA A payload for antimatter matter exploration and light-nuclei astrophysics. Astropart Phys, 2007, 27: 296–315
85 Aguilar M, Alberti G, Alpat B, et al. First result from the alpha magnetic spectrometer on the international space station: Precision measurement of the positron fraction in primary cosmic rays of 0.5–350 GeV. Phys Rev Lett, 2013, 110: 141102
86 Xuhui S. The experimental satellite on electromagnetism monitoring. Chin J Space Sci, 2014, 34: 558–562
87 Alfonsi L, Ambroglini F, Ambrosi G, et al. The HEPD particle detector and the EFD electric field detector for the CSES satellite. Radiat Phys Chem, 2017, 137: 187–192
88 Badoni D, Ammendola R, Bertello I, et al. A high-performance electric field detector for space missions. Planet Space Sci, 2018, 153: 107–119